My first electron density map: A beginner's guide to small angle X-ray diffraction

Ngai Ying Denise Li[1], **Šárka Perutková**[2], **Aleš Iglič**[2] **and Michael Rappolt**[1*]

[1] School of Food Science and Nutrition, University of Leeds, U.K.
[2] Laboratory of Biophysics, Faculty of Electrical Engineering, University of Ljubljana, Slovenia.
[*]E-mail: M.Rappolt@leeds.ac.uk

Abstract. Small angle X-ray diffraction (SAXD) is a non-destructive, analytical method which reveals nanostructural information on the studied material in the form of its electron density distribution, and when applying furthermore peak-shape analysis allows even to retrieve mechanical properties. This technique bases on observing the diffracted intensity of X-rays from a specimen as a function of the scattering angle, *2θ*. Typically, with SAXD it is possible to visualize the sample structure up to a resolution of few Ångströms (1 Å = 10^{-10} m). In this short guide, the main steps of data reduction and analysis are illustrated on a synthetic membrane/water system. The chosen system is 1-dimensional (1D) and centrosymmetric, which keeps the data analysis as simple as possible, but nevertheless all principle steps from data acquisition to the determination of the electron density map are given.

Keywords: Small angle X-ray scattering (SAXS), Small angle X-ray diffraction (SAXD), electron density, Fourier transform, lipid layers

Moja prva določitev prostorske porazdelitve elektronov v snovi s pomočjo meritev sipanja rentgenskih žarkov

V delu so predstavljena navodila za določitev prostorske porazdelitve elektronov in nanostrukturnih podatkov o zgradbi snovi iz izmerjenih spektrov sipane rentgenske svetlobe pod majhnimi sipalnimi koti. Opisana metoda dovoljuje določitev strukture snovi do natančnosti nekaj desetink nanometra. Natančneje je opisana določitev strukture lipidnih plasti umetnih multilamelarnih lipidnih mehurčkov, ki so porazdeljeni v vodi.

1 INTRODUCTION

This beginner's guide to data reduction and analysis for small angle X-ray diffraction (SAXD) data aims to provide a quick and easy approach to understanding the principle steps that have to be taken in order to make the internal nanostructure of the investigated material "visible". The examples provided here are taken from the research field of liquid crystalline matter, and in particular the X-ray scattering from planar lipid membranes will be discussed. The first peak in publications on the electron density maps of different membrane systems was seen in the late 1960s [1-3], when lab X-ray cameras became routinely utilized. Especially lipid/water systems, known for their extraordinary polymorphism, display self-assembled liquid crystalline structures with 1D, 2D or 3D periodicities (for reviews see [4-5]); however, for simplicity and clarity we will concentrate on lamellar membranes only. Lipids are amphiphilic molecules, i.e. exhibit both, hydrophilic and lipophilic functional groups, and once brought into contact with an aqueous solution above a certain threshold concentration (critical micelle concentration), they start to aggregate in such a way that the hydrophilic moieties shield the lipophilic parts from the surrounding water. This process is known as the hydrophobic effect [6], which is an entropy driven process, since the self-assembly of amphiphiles releases bound water. Certainly, the basic element of all biological membranes is the fluid bilayer in which two leaflets of lipids appose each other with their fatty acid chains pointing towards the center of the membrane, whereas the electron dense lipid head groups are found at the membrane-water interface. We note, that the most important structural parameter is the bilayer thickness and in the following we will see how to get hand on this parameter.

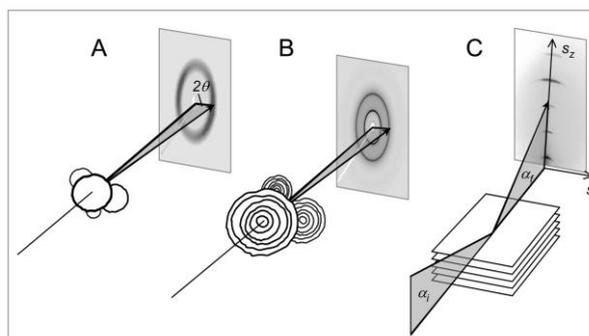In Fig. 1 three different experimental situations are

Figure 1. Typical small angle x-ray scattering cases: (A) diffuse scattering from unilamellar vesicles, (B) powder diffraction from multi-lamellar vesicles, and (C) grazing incidence small angle X-ray diffraction from supported membrane films. The slightly modified figure was taken with permission from [5].

depicted. Bilayers can be organized in unilamellar vesicles (A), in multi-lamellar vesicles (B) or are aligned as solid supported multi-lamellar films[1] (C). Although in all three cases similar lipid bilayer systems are studied, the SAXS patterns differ strongly. The reason is given by the different membrane ordering in space. In the first case, the membranes are uncorrelated, and thus the intensity pattern displays only diffuse scattering, which arises from the electron density fluctuations in the membrane alone. In the latter two cases, the membranes are ordered within stacks on a 1D-lattice, and hence give further rise to diffraction peaks. In panel B the membrane stacks are not oriented, and hence the intensity of each reflection is diffracted on a cone resulting at the detector plane in a so-called Debye-Scherrer ring. In the last case instead, the sample is oriented parallel to a solid support and therefore single diffraction peaks appear along the scattering vector axis s_Z.

In this short review - again for simplicity - we will tackle data sets that display the recorded scattering intensity, *I*, as a function of the scattering vector, *s*, in one dimension only. Please note, that the modulus of the scattering vector, *s*, is not identical but proportional to the scattering angle *2θ* (cp. Fig. 1A). However, this parameter has the great advantage of being universal, i.e. independent of any X-ray source used, as it is normalized by the applied X-ray wavelength, *λ*. Two definitions are commonly used, namely *s* and *q*:

$$s = \frac{q}{2\pi} = \frac{2 \cdot \sin\theta}{\lambda} \qquad (1)$$

The physical background of X-ray scattering will not be given here, but only some few remarks on data acquisition, and the necessary steps of data reduction and data analysis shall illustrate how to retrieve structural information from SAXD experiments. However, the interested reader might find more information in the by now legendary textbooks of Glatter and Kratky [7], and Guinier [8]. Further, we suggest consulting also the comprehensive review of Koch, Vachette and Svergun [9].

2   DATA REDUCTION

Before getting started, a few words shall be said concerning the experimental part. Once the sample is placed into the small angle X-ray camera, mainly two interactions take place in the sample. For instance in water (thickness 1 mm) at a typically applied energy of 8 keV (*λ* = 1.54 Å) the major part of the X-rays gets absorbed (59 %), a big share of photons do not interact at all (37 %), and only a small part gets elastically scattered (4 %). Obviously one is interested to optimize
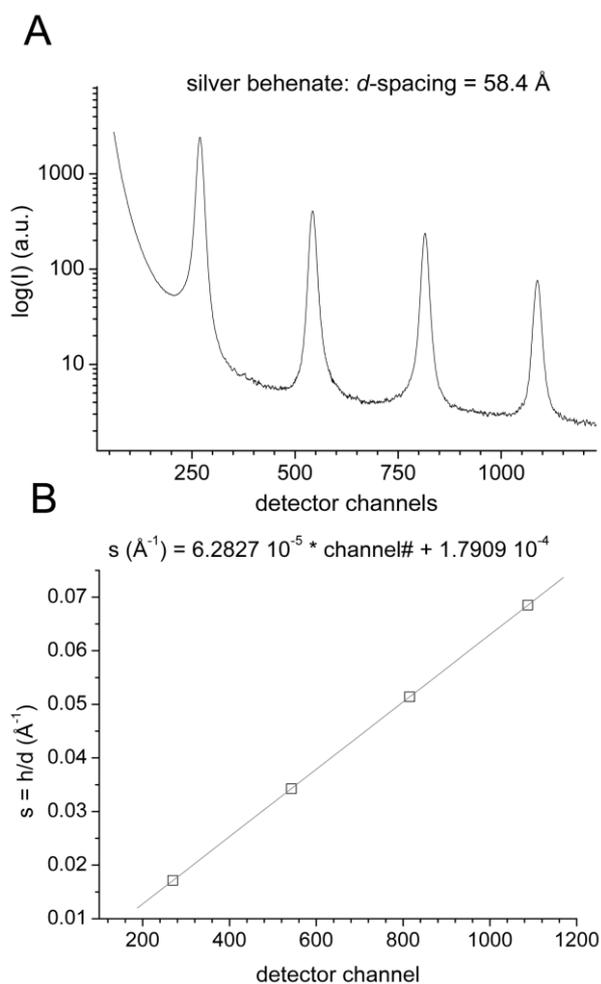

Figure 2. Diffraction pattern of silver-behenate displaying the first 4 diffraction orders (A), and a demonstration of the detector channel calibration with the above diffraction data (B). The lamellar repeat distance of the calibrant is 58.4 Å [11].

the sample thickness such that the scattering event is maximized with respect to absorption. It can be easily shown that at a given wavelength the optimal sample thickness, t_{opt}, depends solely on the linear X-ray attenuation coefficient of the sample, μ_{sample} [9]:

$$t_{opt} = 1 / \mu_{sample}. \qquad (2)$$

Thicknesses deviating greatly from t_{opt} should be avoided, but as a rule of thumb, most soft matter (e.g., polymers and biological material) has an attenuation coefficient close to that of water, which leads to optimum sample thickness of about one millimeter at *λ* = 1.54 Å ($\mu_{water} \approx 1$ mm^{-1}). This in turn enables us to work with relatively small sample volumes of typically 50 µl. Next, one should be aware that not only the SAXD pattern of the sample itself has to be recorded, but also the scattering arising from the background. This usually includes scattering from the sample cell (e.g. capillary) and that of the sample medium (e.g. water). Please note, that especially for weak scattering samples

---

[1]Also single monolayer leaflets are studied, e.g., with Langmuir trough techniques or in rapid cyclic voltametry as well as studies on single supported bilayers are carried out, which will not be discussed in this review.

the background has to be determined with due care in which also corresponding transmission measurements are carried out, and further the sample concentration has to be known (for details see [9]). However, in X-ray diffraction experiments the signal to background ratio is relatively high and often it is sufficient to subtract the background of each diffraction peak in form of second order polynomial.

The first step in the data reduction concerns the calibration of the active area of the detector. The intensity resolution of any detector is either expressed in pixels (2D-detector) or channels (1D-detector). Here, we present data from a 1D detector. In order to obtain a scattering vector scale, the detector channels must be calibrated.

Silver behenate is commonly used to calibrate SAXD patterns. At room temperature in its anhydrous state, it forms lamellar stacks, which give rise to evenly spaced diffraction peaks in the SAXD pattern as shown in Fig. 2 (A). Note, that diffraction represents a special case of elastic scattering, that is, the scattered light is interfering constructively. The geometrical conditions for this constructive interference was first described by William Lawrence Bragg and his father William Henry Bragg in 1913 [10] in response to their discovery that crystalline solids produced patterns of "reflected X-rays". This simple but intriguing geometrical relationship has since long time found its way into various textbooks and for further training, we recommend taking a look for instance into the Encyclopedia Britannica. The condition for diffraction of X-rays is commonly known as Bragg's law and is described in Eq. 3a, where d is the lattice spacing or bilayer thickness, 2θ is the scattering angle (note, incoming and outgoing angle add up to 2θ; cp. Fig. 1C) and n is an integer (1, 2, 3..) describing the order of the diffraction peak. Furthermore, for small angles, $\sin \theta \approx \theta$ and therefore, the equation clearly demonstrates that the scattering angle 2θ is indirectly proportional to the lattice spacing, d, i.e. the scattering pattern is plotted in the reciprocal space.

$$2d \cdot \sin \theta = n\lambda, \tag{3a}$$

and for small θ

$$2\theta \cdot d = n\lambda \quad \Rightarrow 2\theta = \frac{n\lambda}{d} \tag{3b}$$

Now returning to the calibration of our linear 1D-detector, we are routinely using silver behenate (Fig. 2A), which has a known d-spacing of 58.4 Å [11]. In our case we recorded the first 4 orders (n = 1-4) with the known s-values of $s = n/58.4$ Å^{-1}, and hence by simple linear regression we are able to calibrate our s-axis. In the example given the slope was determined to be 3.28 10^{-5} Å^{-1} and the offset 1.79 10^{-4} Å^{-1} (cp. Fig. 2B). Note, that the offset results from the practical circumstance that the zero detector channel never coincides with the direct beam position ($s = 0$).

3   DATA ANALYSIS

Moving on to the experimental data, Fig. 3 displays the diffraction pattern of 1-palmitoyl-2-oleoyl-sn-glycero-3-phosphoethanolamine (POPE) with 3 mol % 1,2-dipalmitoyl-sn-glycero-3-phosphoethanolamine (DPPE) at room temperature in excess of water. Under these conditions the lipids are in the gel-phase, in which all C-C bonds of the fatty acids (palmitic and oleic) are in the *trans*-conformation. These two lipids are commonly found in biomembranes, e.g. the plasma membrane, and dispersed in water form multilamellar vesicles (MLVs; Fig. 1B). MLVs, also known as liposomes, are built up by a number of interlaced spherical vesicles each containing one lipid bilayer. Thus, in radial direction liposomes display a very distinct, 1D-repetition pattern of alternating lipid bilayers and in-between water layers. This 1D-ordered lyotropic liquid crystal diffracts X-rays according to Bragg's law (Eq. 3a) and its SAXD pattern displaying the first four diffraction orders is depicted Fig. 3A. Superimposed, the diffuse background scattering contribution arising from the capillary and the excess of water is also presented (light grey).

It is important to understand that every diffraction peak contains *four different types of information*, which are related to (i) the peak position, (ii) the central peak width, (iii) the peak height and (iv) the peak shape. The first type of information was discussed already above, i.e. d-spacings are deducible from the *peak positions* (Bragg's law). Hence, we can directly determine the d spacing for our demonstration sample from the peak positions $s = n/d$ (this follows from Eq. 1 and 3a). Again applying a linear regression on the measured peak positions $1/d$, $2/d$, $3/d$, $4/d$ and including the direct beam position, 0 (zeroth order), we obtain for our sample a d-spacing of 67.2 Å.

The *central peak width* instead is related to the average crystallite size in a given sample, i.e. in our case to the average number of lamellae within the MLVs. The higher the number of repeating units in the crystallite, the narrower the diffraction peak occurs. This is reflected in the Scherrer equation [12]:

$$FWHM = \frac{0.89 \cdot \lambda}{L} \approx \frac{\lambda}{N \cdot d}, \tag{4}$$

where the full width half maximum (*FWHM*) of the diffraction peak is indirectly proportional to the crystallite size, L, which in our example is equal the average number of membranes in the multilamellar vesicles, N, multiplied with the lattice spacing, d. We note though, that before applying the Scherrer equation, the measured peak profiles of the sample need to be deconvoluted with the direct X-ray beam profile beforehand in order to eliminate the broadening effect that is caused by the X-ray instrument itself. Nonetheless, the final corrected peak width allows to estimate the averaged radius of the MLVs. An excellent review on this topic is given in Chapter 9 of the handbook of Klug and Alexander [13].

Next, each *peak intensity* is related to the electron density contrast with respect to its corresponding lattice periodicity (lattice spacing). For instance, the first diffraction peak intensity ($h = 1$) probes the electron density contrast with a periodicity of d, the second diffraction peak intensity ($h = 2$) probes the electron density contrast with a periodicity $d/2$, and so on. Returning to the diffraction pattern in Fig. 3A, we therefore expect the strongest electron contrast with a repetition length of d, while periodicities of $d/2$ and $d/3$ in the sample display relatively low electron density contrasts. Finally, a medium contrast is observed every $d/4$.

In the following we will demonstrate, how we can exploit our four, measured peak intensities to reconstruct the electron density profile (EDP) of the bilayer stacking of the investigated MLVs. First, we need to fit the intensities (peak areas) of each reflection (Fig. 3B). When dealing with smectic liquid crystalline systems, the reflection *peak-shapes* are reasonably well fitted by Lorentzian distributions. The reason for this lies within the lattice disorder inherent in liquid crystalline systems, which will be discussed in more detail in the outlook of this mini-review. Briefly, while solid crystals display only thermal disorder where the long-range order is conserved (disorder of first type; best to be fitted with Gaussian distributions), the disorder given in liquid crystals is of second type where only a quasi-long range order is given [14, 15]. Note, in thermal disorder the building blocks of a crystal vibrate with respect to the fix lattice points of the crystal, while in liquid crystals each building block undulates with respect to its nearest neighbour.

Finally, in order to obtain the EDP, firstly the reflection intensities must be adjusted by the so-called Lorentz correction. The Lorentz correction is a geometrical correction factor that accounts for the relative differences in the diffraction-probabilities of different crystal planes [15], and usually also considers the given geometry of the instrumental set-up. We note, that in non-orientated, "powder-like" samples, like in our demonstration case, crystal planes with greater d-spacings display relatively higher diffraction-probabilities than those with a smaller d-spacings. For our set-up having utilized an X-ray point source the effective Lorentz correction factor is given by h^2; however, we recommend the interested reader to study the detailed explanations and derivations given by Warren in is his monograph on X-ray diffraction [16]. Secondly, all amplitudes, F_h, which are directly proportional to the probed electron density contrasts need to be calculated from the corrected intensities, ($I_h h_2$), by taking their square root. Now we are prepared to carry out a Fourier transform (Eq. 5) in order to obtain the EDP in radial direction of our MLVs:
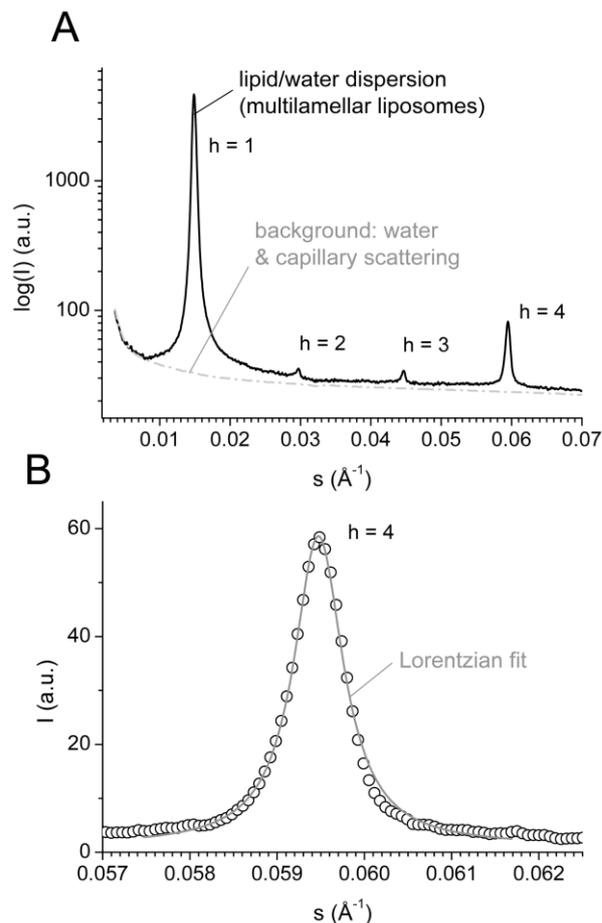
Figure 3. Diffraction pattern of POPE with 3 mol % DPPE at room temperature. The sample is in the gel-phase and the first 4 orders are displayed in panel A and a typical fit of the 4th order reflection is depicted in panel B. The lamellar repeat distance is 67.2 Å.

$$\tilde{\rho}(z) = \sum_{h=1}^{h\,\text{max}} \alpha_h \cdot F_h \cdot \cos\left(2\pi\,s_h z\right)$$
$$= \sum_{h=1}^{h\,\text{max}} \alpha_h \cdot F_h \cdot \cos\left(\frac{2\pi\,h\cdot z}{d}\right), \tag{5}$$

where, F_h, are our experimentally derived amplitudes (form factors), s_h, denotes the peak positions, h gives the peak order (also known as Miller index), α_h are the phase factors of the given amplitudes F_h, and z is the distance in real space. Notice that Eq. 5 only contains a cosine term (no sine term), because for our example, we are dealing with a centrosymmetric structure, which can be perfectly reconstructed by means of using only centrosymmetric, i.e., cosinusoidal electron density contrasts. As a consequence the unknown phases are either $+\pi$ or $-\pi$, and the phase factors $\alpha_h = \cos(\pm\pi)$ can only take the values ± 1. We note, since in X-ray scattering experiments only intensities are recorded, the phase information is not directly obtainable. This problem is known as the 'phase problem' and various strategies have been developed to retrieve this important
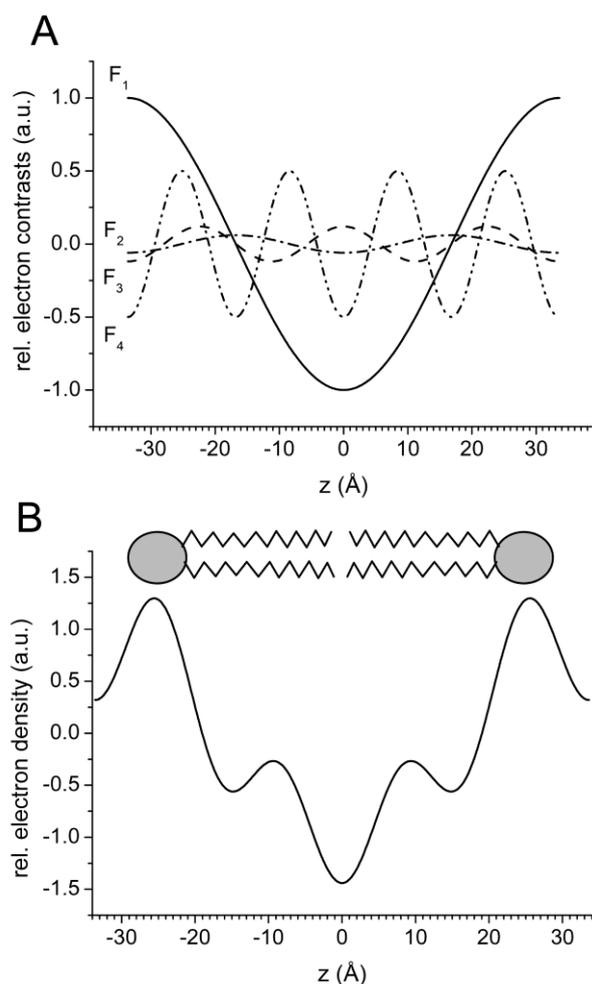
Figure 4. Electron density contrasts (A) and final electron density profile of POPE and DPPE (3 mol%) at room temperature are presented (B). The head-to-head group distance is 51.7 Å.

information needed for the execution of every Fourier transform [7, 16]. However here, for the sake of simplicity the correct phase factors have been taken from literature [17] (see Table 1).

The individual electron density contrasts with the frequencies d, $d/2$, $d/3$ and $d/4$ and with their corresponding amplitudes, F_h, are plotted in Fig. 4A. The summation of these four cosine terms (Eq. 5) leads to the EDP illustrated in Fig. 4B. All structural parameters are summarized in Table 1.

From the obtained EDP, further fine-structural information can be inferred. For example, using the peak-to-peak distance in the EDP, the phosphate-to-phosphate distance in the bilayer is indicated (the highest electron density in the bilayer is given by the phosphate-group of the lipids), which is also referred to as the head-to-head group distance, d_{HH} (see top scheme of Fig. 4B). It is instructive to perform an estimation of d_{HH} and compare it to our experimental result. Since a carbon-carbon bond length accounts for about 1.25 Å [18] and a palmitic fatty acid chain contains 16 carbons,

it follows that the length of two fatty acid chains is equal to 40.0 Å. The diameter of a ethanolamine headgroup is approximately 8 Å [19], and hence an estimation of 48.0 Å for d_{HH} results, which compares well to the result of 51.7 Å deduced from our EDP. Note the slightly higher experimental value might stem from the fact that also oleic fatty acids (C18) are present in the investigated bilayer. Another important parameter concerns the intermembrane water layer thickness, d_W:

$$d = d_W + d_{HH} \tag{6}$$

Inserting our d-spacing and d_{HH} values in Eq. 6 yields to $d_W = 67.2 - 51.7 = 15.5$ Å. Importantly, changes in membrane thicknesses allow to directly monitor the fluidity of lipid bilayers, whereas the intermembrane distances give insight into the balance of repulsive and attractive forces that keep the membrane in place [5].

Summarizing we have shown that an EDP of a lipid bilayer can be reconstructed with four probed electron density contrasts only, and that a Fourier transform in this case study boils down to the sum of four cosine terms. Although we included in our calculation diffraction data limited to $s_{max} = 4/d$, the precision of localizing the phosphate group is about 1 Å [20]. This might be surprising, but Fourier analyzing similar data sets from MLVs and supported lipid films displaying up-to 8 diffraction orders do not significantly change the d_{HH}-values from the fourth order onwards. Higher resolved data sets instead make apparent further structural details in the EDP: for instance, the location of the glycerol backbone and further structural particulars in the fatty acid chains become visible.

Table 1. Structural parameters of the lamellar L_β-phase of POPE with 3 mol% DPPE at room temperature (rf. to Fig. 3).

h	s_h ($Å^{-1}$)	I_h (a.u.)	$I_h\,h^2$ (a.u.)	$\alpha_h \cdot F_h$ (a.u.)
1	0.01488	1.00000	1.0000	-1.00
2	0.02949	0.00094	0.0038	-0.06
3	0.04446	0.00171	0.0154	+0.12
4	0.05949	0.01561	0.2498	-0.50

4   CONCLUSION AND OUTLOOK

The purpose of this beginner's guide to small angle X-ray diffraction was to demonstrate with an easy showcase how nanostructural information can be obtained by applying just some few and simple recipes. The basics to data reduction (calibration and background subtraction) and data manipulation (peak-fitting, Lorentz correction and Fourier analysis) have been discussed in great detail, and when necessary have been complemented by carefully selected references. Our greatest hope is that this guide will inspire the reader to attempt their own first electron density maps and assess their validity.

Our take home message for every beginner should be – apart from demystifying the 'job' to calculate electron densities by Fourier transform – that there are

four distinct portions of information given in the in any diffraction peak: (i) peak positions refer to lattice spacings, (ii) peak widths to crystallite sizes, (iii) peak intensities probe electron density contrasts and (iv) peak shapes reflect the type of crystal-disorder in the sample.

In our case study, the first three parameters are related to the *structure of the bilayers*. Additionally, careful peak-shape analysis allows recovering *mechanical information*. This kind of modelling goes beyond the scope of this mini-review, but we like to stress that novel analysis tools have been constantly developed over the past 15 years allowing to get hold on to on the bilayer bending modulus, K_C, and the bulk compression modulus, B of various membrane systems [21-24].

As a final remark, the biggest intellectual hurdle for every beginner when dealing with scattering methods is that the measured data is displayed in inverse space, while our imagination works properly only in real space. However, with ever-growing computing power and reliable, big databases, we will actually with novel, future setups be able to display electron densities in an *as-soon-as-recorded (ASAR)* fashion. In the time being, we will need to bite into the sour apple and keep on translating inverse space information into real images.

ACKNOWLEDGEMENTS

REFERENCES

[1] Y.K. Levine, A.I. Bailey, M.H. Wilkins. Multilayers of phospholipid bimolecular leaflets. *Nature,* 220, 577-578, 1968.

[2] M.H.F. Wilkins, A.E. Blaurock, D.M.Engelman.. Bilayer Structure in Membranes. *Nature New Biology,* 230,72-76, 1971.

[3] V. Luzzati. X-ray diffraction studies of lipid-water systems. In *Biological membranes*. D. Chapman, editor. Academic Press, New York, 71-123, 1968.

[4] J.M. Seddon. R.H. Templer. Polymorphism of lipid water systems. In *Structure and dynamics of membranes*. R. Lipowsky and E. Sackmann, editors. North-Holland, Amsterdam, 97-160, 1995.

[5] M. Rappolt. The biologically relevant lipid mesophases as "seen" by x-rays. In *Advances in Planar Lipid Bilayers and Liposomes*. A. Leitmannova-Liu, editor. Elsevier Inc., Amsterdam, 253-83, 2006.

[6] C. Tanford. The hydrophobic effect and the organization of living matter. *Science,* 200, 1012-1018, 1978.

[7] O. Glatter, O. Kratky. *Small Angle X-ray Scattering*. Academic Press, London, 1982.

[8] A. Guinier. *X-ray diffraction*. Freeman, San Francisco, 1963.

[9] M.H.J. Koch, P. Vachette, D.I. Svergun. Small-angle scattering: a view on the properties, structures and structural changes of biological macromolecules in solution. *Quarterly Review of Biophysics,* 36, 147-227, 2003.

[10] W.H. Bragg, W.L. Bragg. The Reflexion of X-rays by Crystals. *Proc R. Soc. Lond. A*, 88 (605), 428-38, 1913.

[11] T.C. Huang, H. Toraya, T.N. Blanton, Y. Wu. X-ray powder diffraction analysis of silver behenate, a possible low-angle diffraction standard. *Journal of Applied Crystallography,* 26, 180-184, 1993

[12] P. Scherrer. Bestimmung der Größe und der inneren Struktur von Kolloidteilchen mittels Röntgenstrahlen. *Göttinger Nachrichten,* 2, 98-100, 1918.

[13] H.P. Klug, L.E. Alexander. *X-ray diffraction procedures for polycrystalline and amorphous materials*, John Wiley & Sons, New York, 1974.

[14] R. Hosemann, S.N. Bagchi. *Direct analysis of diffraction by matter*. North-Holland Publ. Co., Amsterdam, 1962.

[15] A.E. Blaurock. Evidence of bilayer structure and of membrane interactions from X-ray diffraction analysis. *Biochimica Biophysica Acta* 650,167-207, 1982.

[16] B.E. Warren. *X-ray Diffraction*. Addison-Wesley, Reading, 1969.

[17] M. Rappolt, A. Hodzic, B. Sartori, M. Ollivon, P. Laggner. Conformational and hydrational properties during the L_β to L_α and L_α to H_{II}-phase transition in phosphatidylethanolamine. *Chemistry and Physics of Lipids,* 154, 46-55, 2008.

[18] A. Seelig, J. Seelig. The dynamic structure of fatty acyl chains in a phospholipid bilayer measured by deuterium magnetic resonance. *Biochemistry*, 13, 4839-4845, 1974.

[19] T.J. McIntosh, S.A. Simon, Area per molecule and distribution of water in fully hydrated dilauroyl-phosphatidylethanolamine bilayers, *Biochemistry*, 25, 4948-4952, 1986.

[20] M. Rappolt. Bilayer thickness estimations with "poor" diffraction data. *J. Appl. Phys.* 107, art.-no 084701. 2010.

[21] G. Pabst, M. Rappolt, H. Amenitsch, P. Laggner. Structural information from multilamellar liposomes at full hydration: Full q-range fitting with high quality x-ray data. *Phys. Rev. E*, 62, 4000-4009, 2000.

[22] M. Rappolt and G. Pabst. Flexibility and Structure of Fluid Bilayer. In *Structure and Dynamics of Membranous Interfaces*. Nag, K. (ed). John Wiley & Sons, Inc., Hoboken, NJ, USA, 2008.

[23] P. Heftberger, B. Kollmitzer, F.A. Heberle, J. Pan, M. Rappolt, H. Amenitsch, N. Kučerka, J. Katsaras, G. Pabst. Global small-angle X-ray scattering data analysis for multilamellar vesicles: the evolution of the scattering density profile model. *J. Appl. Cryst.*, 47 (1), 173-180, 2014.

[24] A. Iglič, V. Kralj-Iglič, D. Drobne. Nanostructures in biological systems: theory and applications. Pan Stanford, Singapore and CRC Press, Boca Raton, 2015.

Ngai Ying Denise Li graduated from Durham University (U.K.) with a Master of Chemistry degree in 2013. Since then she has worked in industry at DuPont Teijin Films, before pursuing a PhD with the SOFI CDT. She is now studying lipid biophysics using X-ray scattering at the University of Leeds, working under Professor Michael Rappolt.

Šárka Perutková received her Master degree from the Faculty of Mechanical Engineering, Czech Technical University in 2008 and her Ph.D. degree from the Faculty of Electrical Engineering, University of Ljubljana in 2013. She received her second Ph.D. from the field of physics at Department of Physics of University of Maribor in 2017. Her research interests include simulations of equilibrium shapes and mechanical stability of biological membranes and lipid nanostructures.

Aleš Iglič received his B.Sc. and Ph.D. degrees in physics and M.Sc. degree in biophysics from the Department of Physics, and the Ph.D. degree in electrical engineering from the Faculty of Electrical Engineering, all from the University of Ljubljana. He is a Full Professor and the Head of Laboratory of Biophysics of the Faculty of Electrical Engineering. His research interests are in electrostatics, biomechanics and statistical physics of biological membranes and interactions of biological systems with inorganic nanostructures.

Michael Rappolt received his Ph.D. (1995) in Physics from the University of Hamburg, Germany. Since April 2013 he is employed at the School of Food Science and Nutrition as Professor of Lipid Biophysics. He is a leading authority on the use of small angle X-ray scattering on investigating the structure and dynamics of lipid membranes. Recent activities have been concentrated on the study of drug/membrane interactions with applications to drug delivery and food.